Available online at www.sciencedirect.com
SCIENCE DIRECT®
International Journal of Heat and Mass Transfer 49 (2006) 1100–1106
International Journal of HEAT and MASS TRANSFER
www.elsevier.com/locate/ijhmt

High resolution measurements of wall temperature distribution underneath a single vapour bubble under low gravity conditions

Christof Sodtke, Jürgen Kern, Nils Schweizer, Peter Stephan *

Chair of Technical Thermodynamics, Darmstadt University of Technology, Petersenstrasse 30, D-64287 Darmstadt, Germany

Received 14 September 2004; received in revised form 11 July 2005
Available online 3 November 2005

Abstract

Heat transfer performance in nucleate boiling crucially depends on a circular thin film area near the foot of a vapour bubble where high heat fluxes and thus high local evaporation rates occur. The corresponding wall temperature drop close to the tiny thin film area is computed using an existing nucleate boiling model. To verify the predicted temperature distribution, an experiment is designed with a thin electrically heated wall featuring two-dimensional, high resolution temperature measurement using unencapsulated thermochromic liquid crystals. By means of temperature measurements during a parabolic flight under low-g conditions, the validity of the model used to calculate the temperature distribution in the tiny thin film area could be confirmed.

Keywords: Microscale; Thermochromic liquid crystals; Low gravity; Nucleate boiling; Interline region; Micro-region

1. Introduction

High performance heat transfer devices or processes, such as heat pipes, capillary pumped loops, spray cooling or nucleate boiling, achieve very high heat fluxes due to evaporation at thin liquid films. A considerable amount of the total heat supplied to the system passes through a tiny thin liquid film area where the liquid-vapour interface approaches the wall material (Fig. 1).

In this ''interline region'' [1] or ''micro-region'' [2], the curvature of the liquid–vapour interface differs strongly from the mean curvature in the liquid bulk (''macro-region''). Adhesion forces between liquid and wall cause a steady transition of the meniscus into a flat adsorbed, non-evaporating film. The curvature change and the adhesion forces cause a pressure gradient in the liquid that leads to a transverse liquid flow from the bulk of the liquid to the thin film region. Additional effects that are triggered in the micro-region are the interfacial thermal resistance and concentration effects (if mixtures are used), such as a local variation of phase equilibrium as well as Marangoni convection. Considering these special phenomena in equations for mass, momentum, and energy transfer, modelling equations for the micro-region are obtained that can be solved numerically in an iterative process together with a standard model for the macro-region heat transfer as done by several researchers, e.g. for heat pipes [2,3] or nucleate boiling [4–6]. These models have been verified on a macroscopic scale only, e.g. by comparing computed with measured heat transfer coefficients, because the typical length scale of the micro-region is of the order of 10^{-6} m. To still get an evaluation of computed micro-region data the authors applied a high resolution temperature measurement technique using unencapsulated thermochromic liquid crystals (TLCs) to nucleate boiling at a single artificial cavity under low-g. The low-g environment where the vapour bubbles are largely undeformed and detach with low frequencies from the heated wall greatly facilitated experiments.

* Corresponding author. Tel.: +49 6151 16 3159; fax: +49 6151 16 6561.
E-mail address: pstephan@ttd.tu-darmstadt.de (P. Stephan).

0017-9310/$ - see front matter © 2005 Elsevier Ltd. All rights reserved.
doi:10.1016/j.ijheatmasstransfer.2005.07.054

Nomenclature

d_{sub}	diameter of the subsystem (m)
HSV	hue, saturation, value
hue	scalar colour value (degrees)
p	pressure (N/m^2)
q'''	heat flow density in wall (W/m^3)
r	radius (m)
RGB	red–green–blue colour triples
t	temperature (K)
TLC	thermochromic liquid crystal
x	co-ordinate of measurement area (m)

Greek symbols

η	co-ordinate normal to the wall (m)
τ	time (s)
ξ	co-ordinate parallel to the wall (m)

Subscripts

ads	adsorbed film
sat	saturation

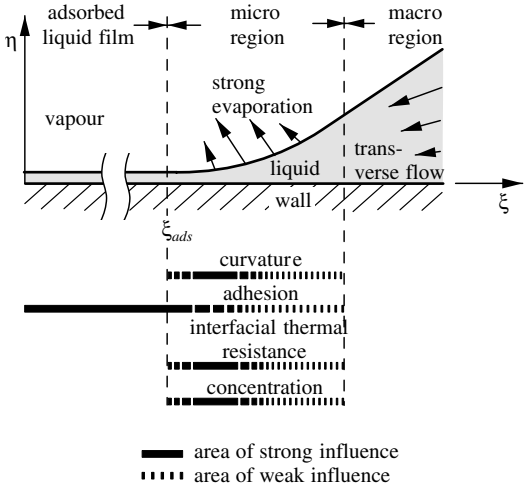

Fig. 1. Significant phenomena in the micro-region.

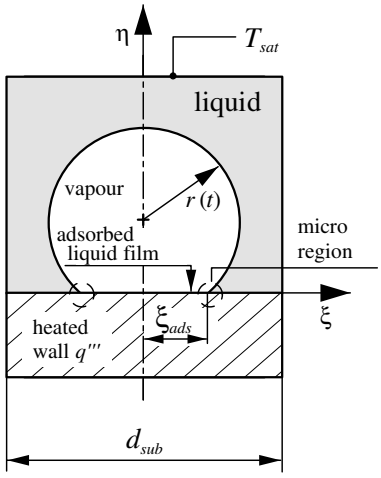

Fig. 2. Single bubble subsystem.

In Section 2, the theoretical nucleate boiling model is briefly described and the calculated wall surface temperature distribution is shown. This temperature is a very sensitive result of the model and therefore a good one for comparison with experimental results. In Section 3, the measurement technique using unencapsulated TLCs and in Section 4 the experimental set-up are described. Finally, in Section 5 the temperature data obtained from experiments is presented, discussed, and compared with the calculated data to evaluate the model.

2. Nucleate boiling model

A detailed description and verification of the presented model can be found in [6]. Thus only a brief description is given in this section.

The model describes heat and mass transfer in a single bubble subsystem for the time period when the bubble is growing from an infinitesimal size to the departure radius (Fig. 2). The subsystem consists of a single vapour bubble, surrounding liquid, and a part of the heated wall. Using cylindrical co-ordinates (ξ, η), the diameter d_{sub} of the single bubble subsystems corresponds to the bubble site density, i.e. the subsystem can be used to model nucleate boiling in technical evaporators. Since the model is based on the assumption that growing bubbles do not interact, it is valid for low and intermediate heat fluxes. To calculate heat and mass transfer in the subsystem, microscopic effects are considered in the micro-region (Fig. 2) as described in Section 1.

For evaluation of the micro-region model, the temperature distribution on the heater surface is calculated. In accordance with the performed measurements nucleate boiling of FC-72 on stainless steel at 0.7 bar is chosen and a constant volumetric heat generation within the wall is assumed. The side of the heating foil pointing towards ambient is considered adiabatic. In Fig. 3 the calculated wall temperatures at the surface ($\eta = 0$) of the single bubble subsystem (Fig. 2) are illustrated. Due to very high local evaporation rates in the micro-region (heat flux in the micro-region is up to 100 times higher than in the macro-region [6]), the wall temperature drops in the vicinity of the micro-region.

The minimum temperature corresponds to the computed wall temperature in the micro-region (Fig. 3).

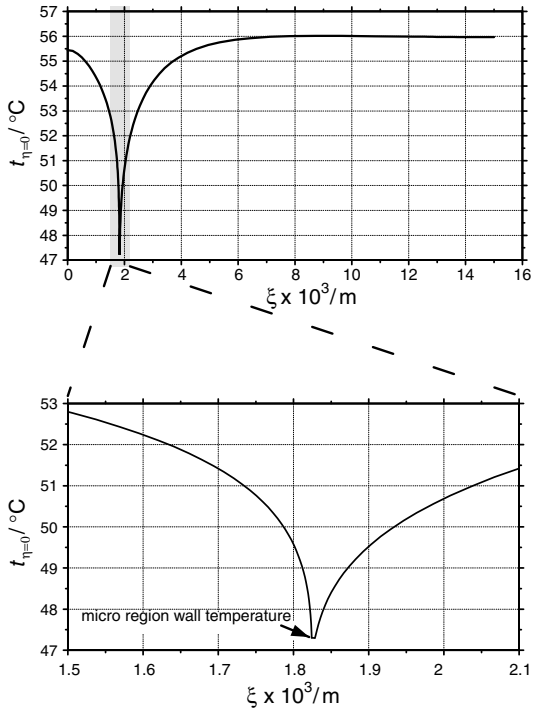

Fig. 3. Calculated surface temperature of the wall (FC-72 on stainless steel, $p = 0.69 \times 10^5$ N/m^2, $q''' = 10^9$ W/m^3, $d_{sub} = 30 \times 10^{-3}$ m, $r = 5 \times 10^{-3}$ m, $\xi_{ads} = 1.82 \times 10^{-3}$ m).

3. Microscale temperature measurements

The extremely small spatial dimension of the region to be investigated triggers several problems for measurements (e.g., the smallest available thermocouples are still one or two orders of magnitude bigger than the dimension of the micro-region itself). Therefore, to measure the strong wall temperature drop close to the tiny micro-region (Fig. 3), unencapsulated TLCs are used that feature a high spatial and temporal resolution. Since they cannot be used on the surface where nucleate boiling takes place they are applied on the backside of a thin (thickness 10×10^{-6} m) foil that is used instead of a thick wall. The foil is electrically heated with constant voltage and current, resulting in a constant heat flow density in the foil. Due to the very low thickness of the foil the temperature distribution on the back of the foil deviates only little from that on the front of the foil. This has already been shown for a similar capillary slot experiment where the same foil has been used [7].

TLCs reflect a distinct colour depending on their temperature when illuminated by white light. Below and above their active temperature range they are transparent, within their working range the reflected light changes from red to green to blue with increasing temperature. With TLCs in the unsealed form, an almost continuous layer can be achieved even on the microscopic scale. Furthermore, they can be applied in a thinner layer than encapsulated crystals giving brighter colours and a smaller temperature drop across the layer [8]. However, the performance of unsealed

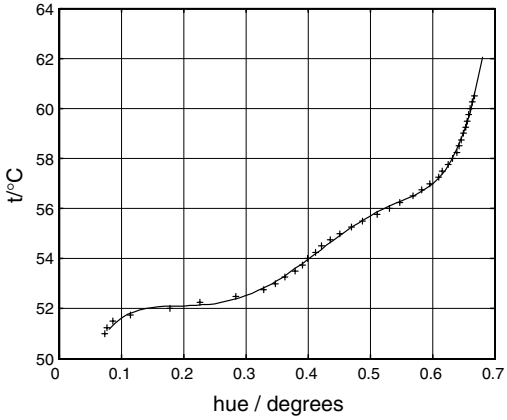

Fig. 4. Typical calibration curve with seventh-order regression.

TLCs deteriorates quickly in the presence of oxygen, solvents or lubricants.

For quantitative temperature measurements an image of the TLCs is captured and the colour information is converted from the RGB-signal of the camera to the HSV-colourspace (hue, saturation, value). In the HSV-colourspace, the hue-value is measured in degrees. It contains all the colour information and can therefore be used as a single value for the temperature measurement.

An 'in situ' calibration method for the TLCs has been developed, where the TLCs can be calibrated within the experimental set-up. The temperature of the TLCs can be controlled with a thermostat. By measuring the temperature of the TLCs with thermocouples and recording their colourplay a correlation of hue-value and temperature can be obtained. A seventh-order regression proved to be a good approximation for the correlation. A typical calibration curve is shown in Fig. 4.

Measurements have been conducted showing a mean temperature uncertainty of 0.5 °C for a single pixel without spatial filtering [9]. The response time of encapsulated TLCs is about 3×10^{-3} s [10]. Values of unencapsulated TLCs are not available in the literature, but the response time of unencapsulated TLCs is lower than the response time of encapsulated TLCs due to thermal inertia of the encapsulation material. A response time of 3×10^{-3} s or lower is sufficient for the temperature measurements of wall temperature distribution in the presented experiment that was carried out in a parabolic flight under low-g conditions where the transient process is slower than under 1 g conditions.

4. Experimental set-up

To study the wall temperature distribution close to a single FC-72 vapour bubble the experimental set-up described in the following paragraph is used.

As shown in Fig. 5, the test cell consists of a hollow Plexiglas cylinder, an aluminium bottom plate and a thin electrically heatable stainless steel foil (2.8×10^{-2} m $\times 4.2 \times 10^{-2}$ m) as top cover with TLCs applied on the backside.

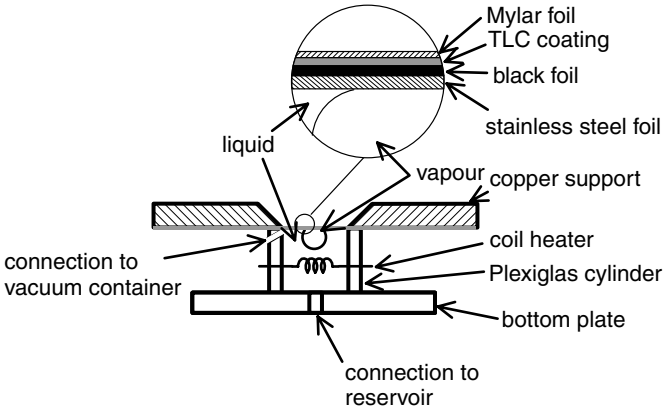

Fig. 5. Schematic of test cell.

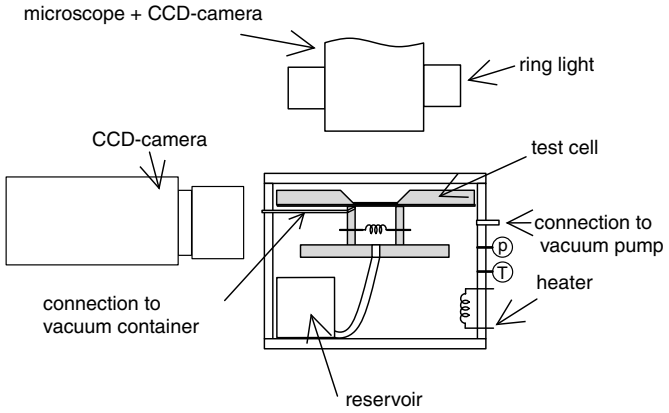

Fig. 6. Schematic of experimental set-up.

The Plexiglas cylinder is filled with the working fluid FC-72. The volume of the cylinder is kept small to reduce inertia effects during the change from 1.8 g to 0 g of a parabolic flight [11]. The stainless steel foil has a thickness of 10×10^{-6} m and is used as a resistance heater powered by DC-current. It is equipped with an artificial nucleation site created by spot welding on the side pointing inside the fluid chamber to facilitate the formation of a single vapour bubble at a specific position, so that the bubble grows towards the base plate in the Plexiglas cylinder. The very thin foil and a high resolution TLC-coating applied on a thin black tape are used so that the measured temperature distribution on the backside of the foil shows only a small variation from the temperature signal at the front side where the evaporation takes place [7].

The backside of the foil is coated with a 5×10^{-6} m thin black tape (*Alfac GmbH*, *Al 109*) on top of which non-encapsulated TLCs are applied using a brush. The TLC-layer has an approximate thickness of 10×10^{-6} m. A transparent Mylar-sheet (*Pütz GmbH + Co. Folien KG*) protects the TLC coating. The stainless steel foil is supported by a copper structure which was coated by a thin layer of paint to guarantee electrical insulation.

The test cell has an inlet for liquid supply from an external compressible liquid reservoir and a connection to a vacuum container for removal of vapour. A heating coil is located close to the bottom plate of the test cell to control the subcooling of the liquid.

Both test cell and the liquid reservoir are located in a Plexiglas container (see Fig. 6) inside which the pressure can be varied using a vacuum pump. That way, the saturation temperature of the FC-72 can be adjusted to fit the working range of the TLCs. A heater inside the container is used to preheat the working fluid and the test cell and to reduce heat losses from the test cell to its surrounding. Temperature and pressure inside the Plexiglas container are measured using a pressure transducer and several thermocouples.

To measure the wall temperature distribution at the foot of the growing vapour bubble, the colourplay of the TLCs is recorded through the wall of the Plexiglas container with a long-working-distance microscope and a three-chip CCD-camera. A ring light connected to a cold light source is used for coaxial illumination of the TLCs. The camera is connected to a framegrabber card in a PC that captures the images as RGB-matrices. The captured images are then processed using MATLAB to convert the TLC-images into temperature profiles. Using the microscope the field of view of the camera is 800×10^{-6} m $\times 600 \times 10^{-6}$ m, for the camera this results in a spatial resolution of 1.04×10^{-6} m/pixel. Temperatures are measured along lines with arbitrary starting and ending points. To eliminate noise the temperature is averaged over a ten pixel wide band orthogonal to the chosen line.

A second CCD-camera is installed to record the shape of the vapour bubbles from the side. The Plexiglas container, the CCD-cameras, the computer, vacuum pump, and the necessary power supplies are fixed in a rack that can be used inside the Airbus A 300-ZERO-G of the European Space Agency (ESA) [11].

5. Results

With the set-up described above, high spatial resolution temperature measurements were conducted on ground and on board of the ESA A 300-ZERO-G airplane.

Before each experiment the working fluid was carefully degassed by first reducing the pressure inside the Plexiglas container and then heating the FC-72 up until boiling occurred. Any vapour formed in the reservoir and test cell was removed. This procedure was repeated periodically several times. Before each measurement, the fluid in the test cell was heated close to saturation temperature so that the subcooling of the bulk liquid was kept between 3 °C and 5 °C.

In the case of measurements under low-g conditions all vapour was removed from the test cell prior to entering the low-g phase by opening the valve to the vacuum container. Then the current to the heating foil was switched on and a vapour bubble was created at the nucleation site in the low-g environment. TLC-images were taken manually when the effect of the micro-region could be seen inside the field of

view of the CCD-camera. The position of the camera was adjusted and therefore the co-ordinate x of the captured pictures is not the same as the co-ordinate ξ used in the nucleate boiling model. After each parabola, in the 1.8 g and 1 g phase of the flight, the vapour was removed from the test cell by opening the valve to the vacuum container. However, it could also be observed that the vapour bubbles completely condensed quickly after the heating power was reduced indicating that the FC-72 was well degassed. After a set of 30 parabolas the TLCs were calibrated.

For the ground measurements, the experimental procedure was similar. The calibration of the TLCs was done after 10 sets of measurements.

5.1. Ground measurements

On ground, the vapour bubble created by evaporation at the nucleation site is strongly deformed as shown in Fig. 7a, bottom picture. Therefore the bubble grows relatively fast towards the Plexiglas cylinder which means the micro-region also moves fast. Due to the fast motion of the micro-region, the heat input to the bubble had to be kept comparatively low to be able to capture images of the TLCs. The colourplay of the TLCs and the temperature profile can be seen in Fig. 7a. Due to the high spatial resolution of the long-working-distance microscope in connection with the CCD-camera, only a section of the circular contact line can be captured in the images. The area of the adsorbed film at the heated wall of the bubble is located in the lower right corner of the colourplay, while the upper left corner shows the area of the liquid bulk of the bubble. The colour data is transferred into temperature data along a line, as indicated by the white arrow from the liquid bulk to the adsorbed film of the bubble. The heat input for the ground experiment is 3.2 W (2.13×10^8 W/m^3).

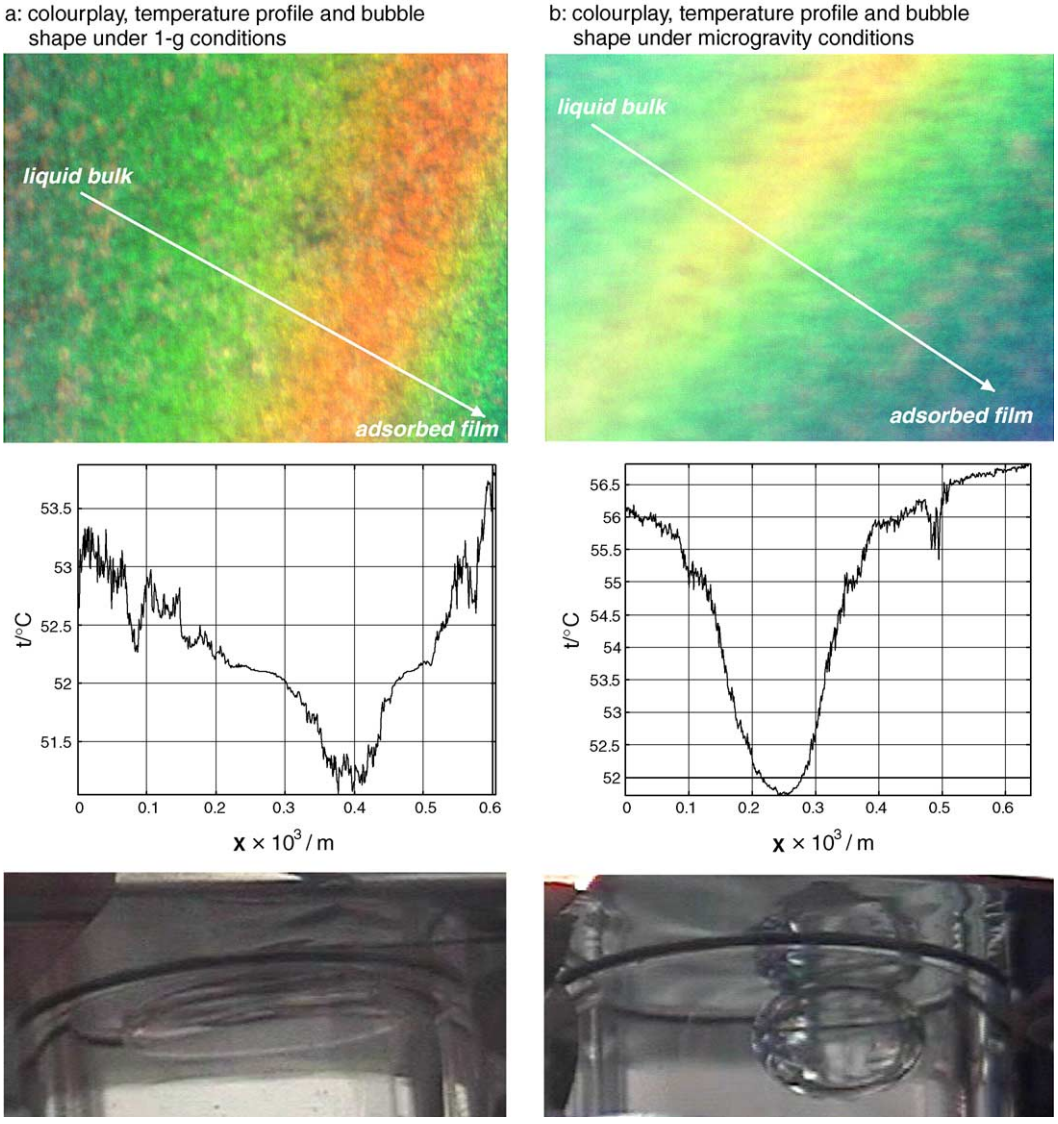

Fig. 7. Experimental results for 1-g (heat input: 3.2 W, 2.13×10^8 W/m^3) and low-g (heat input: 15 W, 1000 W/cm^3) environments.

5.2. Low-g measurements

Bubbles created in low-g conditions are more spherical in shape as shown in Fig. 7b, bottom picture. When the bubble grows, it does so isotropically in all three dimensions, which causes the micro-region to move slower along the heating foil compared to the bubble growth in a 1 g environment at the same heat input. Therefore a higher heat input of 15 W (10^9 W/m^3) is measured under low-g conditions as shown in Fig. 7b. The colourplay of the TLCs, the corresponding temperature profile, and the shape of the bubble can be seen in Fig. 7b. The TLC-image displayed shows the area of the adsorbed film of the bubble on the right hand side of the picture and the temperature is measured as indicated by the white arrow from the area of the liquid bulk to the area at the adsorbed film of the bubble. The wall temperatures of the adsorbed film of the bubbles are higher than the ones at the liquid bulk of the bubble due to the presence of the adsorbed film. Heat is generated homogeneously in the heating foil, but the heat flow through the adsorbed film tends to zero which causes the temperature to rise.

Several temperature measurements have been conducted in the low-g environment. Depending on heating power and g-jitter [12], the temperature drop caused by the micro-region changes. The temperature profiles for two different sets of measurements can be seen in Figs. 8 and 9. The width of the temperature drop caused by the micro-region varies between 0.1×10^{-3} m and 0.2×10^{-3} m, while the range of the heating power is 12–15 W.

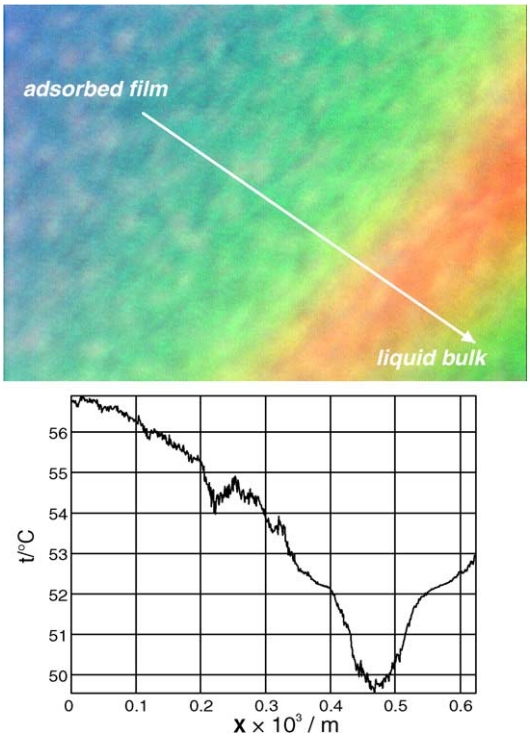

Fig. 8. Experimental result of low-g measurement (heat input: 15 W, 10^9 W/m^3).

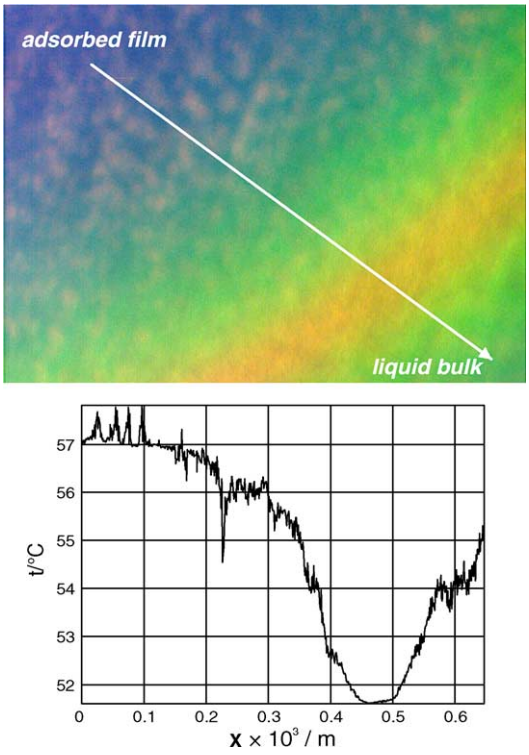

Fig. 9. Experimental result of low-g measurement (heat input: 12 W, 8×10^8 W/m^3).

A comparison of the low-g measurements and the numerical calculations (see Section 2 for details and assumptions) is shown in Fig. 10 (co-ordinates x and ξ are fitted according to the temperature drop in the micro-region). The measured and computed temperature distribution agree qualitatively. Quantitatively computed temperatures are approximately 2 °C lower than measured temperatures. Using TLCs the error of measurement is 0.51 °C (see Section 3). Additionally, the power input to the heating foil was measured manually using an analog voltmeter and an analog amperemeter. The readings of these devices show rather big errors in power input of approximately 20%. A variation of ±20% in power input leads to a shift of ±2.4 °C in computed wall temperatures. The effects of uncertainty due to other measured data on the computation are negligible compared to the uncertainty in the power measurement. Therefore, the

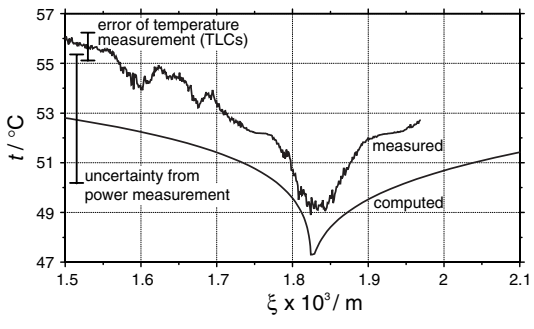

Fig. 10. Comparison of computed and measured (low-g) wall temperature distribution close to the micro-region (conditions as for Fig. 3).

numerical results may also agree quantitatively with the measurements.

6. Summary and conclusions

A theoretical model to calculate nucleate boiling heat and mass transfer is briefly summarised. The model includes microscopic heat and mass transfer phenomena in a wedge shaped micro-region where the liquid–vapour phase interface approaches the wall material. To verify the model on a microscopic scale the wall temperature distribution close to the micro-region is computed and compared to measured data from experiments. The corresponding experimental set-up is described and results of the performed measurements under low-g are presented. By means of unencapsulated thermochromic liquid crystals it was possible for the first time to obtain a high resolution wall temperature distribution close to the micro-region of a vapour bubble in nucleate boiling. The results show a strong wall temperature drop close to the micro-region and thus confirm the existence of this region. The measured temperature data was further used to verify the nucleate boiling model on a microscopic scale.

Acknowledgements

The authors wish to acknowledge the support from Novespace, France, and the European Space Agency (ESA) through the 37th ESA Parabolic flight campaign and the CIMEX research program. We also thank 3M Deutschland GmbH for providing us with the test fluid FC-72.

References

[1] S. DasGupta, I.Y. Kim, P.C. Wayner, Use of the Kelvin–Clapeyron equation to model an evaporating curved microfilm, ASME J. Heat Transfer 116 (1994) 1007–1015.
[2] P. Stephan, C.A. Busse, Analysis of the heat transfer coefficient of grooved heat pipe evaporator walls, Int. J. Heat Mass Transfer 35 (1992) 383–391.
[3] A. Faghri, Heat Pipe Science and Technology, Taylor & Francis, Washington, 1995.
[4] P. Stephan, J. Hammer, A new model for nucleate boiling heat transfer, Heat Mass Transfer 30 (1994) 119–125.
[5] V.K. Dhir, Numerical simulations of pool-boiling heat transfer, AIChE J. 47 (2001) 813–834.
[6] J. Kern, P. Stephan, Theoretical model for nucleate boiling heat and mass transfer of binary mixtures, ASME J. Heat Transfer 125 (2003) 1106–1115.
[7] C. Höhmann, Temperaturmessverfahren zur räumlich hochauflösenden Untersuchung des Wärmetransports an einem verdampfenden Flüssigkeitsmeniskus, PhD thesis, Darmstadt University of Technology, Darmstadt, 2004.
[8] M. Aligoodarz, Y. Yan, D. Kenning, Wall temperature and pressure variations during flow in narrow channels, in: Proceedings of the 11th International Heat Transfer Conference, Kyongju, 1988, pp. 225–230.
[9] C. Höhmann, P. Stephan, Microscale temperature measurement at an evaporating liquid meniscus, J. Exp. Thermal Fluid Sci. 26 (2002) 157–162.
[10] P.T. Ireland, T.v. Jones, The response time of a surface thermometer employing encapsulated thermochromic liquid crystals, J. Phys. 20 (1987) 1195–1199.
[11] Available from: <http://www.novespace.fr>.
[12] P. Di Marco, W. Grassi, G. Memoli, T. Takamasa, A. Tomiyama, S. Hosokama, Influence of electric field on single gas-bubble growth and detachment in microgravity, Int. J. Multiphase Flow 29 (2003) 559–578.